International Journal of Concrete Structures and Materials
Vol.9, No.3, pp.369–379, September 2015
DOI 10.1007/s40069-015-0112-9
ISSN 1976-0485 / eISSN 2234-1315

Estimation of Friction Coefficient Using Smart Strand

Se-Jin Jeon[1),*], Sung Yong Park[2)], Sang-Hyun Kim[1)], Sung Tae Kim[2)], and YoungHwan Park[2)]

(Received June 19, 2015, Accepted August 18, 2015, Published online September 11, 2015)

Abstract: Friction in a post-tensioning system has a significant effect on the distribution of the prestressing force of tendons in prestressed concrete structures. However, attempts to derive friction coefficients using conventional electrical resistance strain gauges do not usually lead to reliable results, mainly due to the damage of sensors and lead wires during the insertion of strands into the sheath and during tensioning. In order to overcome these drawbacks of the existing measurement system, the Smart Strand was developed in this study to accurately measure the strain and prestressing force along the strand. In the Smart Strand, the core wire of a 7-wire strand is replaced with carbon fiber reinforced polymer in which the fiber Bragg grating sensors are embedded. As one of the applications of the Smart Strand, friction coefficients were evaluated using a full-scale test of a 20 m long beam. The test variables were the curvature, diameter, and filling ratio of the sheath. The analysis results showed the average wobble and curvature friction coefficients of 0.0038/m and 0.21/radian, respectively, which correspond to the middle of the range specified in ACI 318-08 in the U.S. and Structural Concrete Design Code in Korea. Also, the accuracy of the coefficients was improved by reducing the effective range specified in these codes by 27–34 %. This study shows the wide range of applicability of the developed Smart Strand system.

Keywords: friction coefficient, fiber Bragg grating sensor, prestressing tendon, strand, sheath, duct, prestressed concrete structure.

1. Introduction

The calculation and control of elongation and the prestressing force during tensioning of tendons are of primary importance in post-tensioned concrete structures. In this respect, the friction that occurs through the interaction between strands and a sheath during tensioning in a post-tensioning system has a significant effect on the distribution of prestressing force and elongation of tendons. Underestimation or overestimation of the friction coefficients can lead to unexpected structural behavior in terms of camber, deflection, and stress distribution (ACI 2014). Although the relevant design codes and specifications recommend that the friction coefficients be experimentally determined (ACI 2014; KCI 2012), the set-up of test specimens and measurement of forces or strains of tendons required to obtain the coefficients are not easy to carry out. Furthermore, the accuracy of the coefficients is not always guaranteed because of a number of variables affecting the coefficients while testing. Therefore, the friction coefficients that are specified in design codes and specifications are still referred to frequently. However, the coefficients show a wide range of differences depending on the provisions, and are sometimes expressed as a range rather than as a specific value. This has caused some confusion and trial-and-error practices for designers and constructors, and has led to the inconsistent use of friction coefficients. An acceptable error limit of ±5 or ±7 % of the jacking force between the measured value in a jack and the calculated value from the elongation of tendons (AASHTO 2014; ACI 2014) may still provide a source of discrepancy from the original calculation sheet in the stress distribution of concrete as well as tendons.

In order to reasonably determine the friction coefficients, a number of studies have been performed, but a standard method has not yet been established (Gupta 2005; Jeon et al. 2009; Jeung et al. 2000; Kitani and Shimizu 2009; Moon and Lee 1997). It is found that in each method, some assumptions have been made and that each method depends on inaccurate or incomplete data. In particular, attempts made to derive friction coefficients using conventional electrical resistance strain gauges do not seem to lead to reliable results, mainly due to the damage of sensors and lead wires during the insertion of strands into a sheath and during tensioning as well as the difficulty of gauge installation on a strand. Although a load cell can be installed on the dead end of the test specimen in the opposite side of the live end that is subjected to jacking, the load cell can only provide additional information on the prestressing force at

[1)]Department of Civil Systems Engineering, Ajou University, Suwon-si, Gyeonggi-do 443-749, Korea.
*Corresponding Author; E-mail: conc@ajou.ac.kr
[2)]Structural Engineering Research Institute, Korea Institute of Civil Engineering and Building Technology, Goyang-si, Gyeonggi-do 411-712, Korea.

the dead end, which is not sufficient to determine the exact distribution of prestressing force required to derive reliable friction coefficients.

In order to overcome these drawbacks of the existing measurement system, the Smart Strand with the embedded fiber Bragg grating sensors was developed in this study to accurately measure the strain and prestressing force along the strand (KICT 2013; Kim et al. 2015). As one of the applications of the Smart Strand, friction coefficients were evaluated using a full-scale test of a 20 m long beam. The obtained friction coefficients were compared with those specified in current provisions for verification and, as a result, several improvements were proposed.

2. Friction Coefficients

2.1 Friction in Post-tensioning System

While the prestressing tendons are tensioned using a jack, the loss of prestress occurs along the tendons due to the friction between the tendons and the sheath in a post-tensioning system. Figure 1 demonstrates two major types of friction. Curvature friction is induced at the curved section of a sheath, where the tendons come into contact with the sheath during tensioning. On the other hand, wobble friction occurs even in a straight sheath due to the unintended deformation of the sheath during handling or casting of concrete, although the sheath is supported at a certain interval before casting.

The predictive equation of the prestressing force as affected by the friction can be derived as shown in Eq. (1) (Nilson 1987).

$$P_{x1} = P_{x2}e^{-(\mu\alpha+kl)} \tag{1}$$

where P_{x1} and P_{x2} are the prestressing forces at the points of $x1$ and $x2$ on a tendon, respectively, with $x2$ closer to the tensioning point, μ is the curvature friction coefficient, k is the wobble friction coefficient, α is the variation of angle between $x1$ and $x2$, and l is the distance between $x1$ and $x2$.

2.2 Friction Coefficients in Provisions

The friction coefficients specified in various codes, specifications, and manuals, etc. are summarized and compared in Table 1. It is noted that some provisions provide different friction coefficients according to the type and surface condition of the prestressing steel and sheath. Although Table 1 represents the case of strands in a galvanized metal sheath that is most frequently used worldwide, it still shows a wide range of variation of the values from provision to provision, and even in a single provision. For the wobble friction coefficient, the lowest value is 0.00066 as specified in several American provisions (AASHTO 2002; AASHTO 2014; Caltrans 2005; PCI 2011), whereas the highest value is 0.0066 as presented in the Korean design codes (KCI 2012; KRTA 2010) and the previous ACI 318 code (ACI 2008). The difference is as much as ten times. On the other hand, most of the curvature friction coefficients fall into the range of 0.15–0.25, with the recommended value of around 0.20, except for the exceptionally high value specified in the Japanese specifications (JRA 2012; JSCE 2007).

Therefore, a number of attempts have been made to develop more reasonable friction coefficients. However, in several studies, one of the two types of friction coefficients was assumed, while the other friction coefficient was evaluated (Kitani and Shimizu 2009; Moon and Lee 1997); this involves an intrinsic inaccuracy that is strongly affected by the initial assumption of the value of a friction coefficient. The errors that may be induced by this type of methodology were analyzed in some studies (Park and Gil 2004; Park and Kang 2003). Some studies referred to the strains measured by the conventional electrical resistance strain gauges attached to the surface of a strand (Jeung et al. 2000). It is generally accepted, however, that the reliability of the strains obtained by this method is somewhat questionable due to a number of sources of uncertainty and inaccuracy. Gupta (2005) developed a technique to measure the prestressing force at any point of a strand using a tension tester based on the relationship between the lateral deflection and tension of the strand. However, it may be regarded that this method uses an indirect measurement of tension, which possibly involves some errors. Therefore, a more reliable methodology is required to derive realistic friction coefficients in terms of acquirement of the actual strain distribution of a strand and evaluation of the friction coefficients using the measured data.

3. Principle of Smart Strand

Usually, 7-wire strands with a nominal diameter of 12.7 or 15.2 mm are used as prestressing tendons in prestressed concrete (PSC) structures (ASTM 2012; KATS 011). These prestressing tendons consist of one core wire and six outer helical wires made of steel as shown in Fig. 2a. When the strain distribution along a strand needs to be measured, in most cases, the only possibility has been to attach the usual electrical resistance strain gauges on the helical wires exposed outside; although it is desirable to install sensors in the straight core wire to minimize the damage caused by the contact between the strands and between the strand and the sheath. Moreover, the strain measured from this gauge does

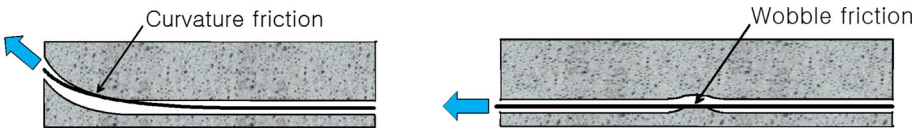

Fig. 1 Friction in a post-tensioning system.

Table 1 Recommended friction coefficients.

Provisions	Wobble friction coefficient, k (/m)	Curvature friction coefficient, μ (/radian)
Structural concrete design code (KCI 2012)	0.0015–0.0066	0.15–0.25
Design code for highway bridges (KRTA 2010)	0.0015–0.0066	0.15–0.25
ACI 318-08 (ACI 2008)	0.0016–0.0066	0.16–0.25
ACI 318-14 (ACI 2014)	Not specified	
Standard specifications for highway bridges (AASHTO 2002)	0.00066	0.15–0.25
AASHTO LRFD bridge design specifications (AASHTO 2014)	0.00066	0.15–0.25
Bridge design manual (PCI 2011)	0.00066	0.20
Post-tensioning manual (PTI 2006)	0.0010–0.0023 (Recommended value: 0.0016)	0.14–0.22 (Recommended value: 0.18)
Prestress manual (Caltrans 2005)	0.00066	0.15, 0.20, 0.25, etc. (Related to the length of a strand)
Canadian highway bridge design code (CSA 2006)	0.003, 0.005 (Related to the diameter of a sheath)	0.20
BS 8110 (BSI 1997)	Not less than 0.0033	0.20, 0.25, 0.30 (Related to rust)
Eurocode 2 (CEN 2002)	0.00095–0.0019	0.19
CEB-FIP model code (CEB 1993)	0.00095–0.0019	0.19
fib model code for concrete structures (fib 2013)	0.0008–0.002	0.16–0.20
Standard specifications for concrete structures (JSCE 2007)	0.004	0.30
Specifications for highway bridges (JRA 2012)	0.004	0.30

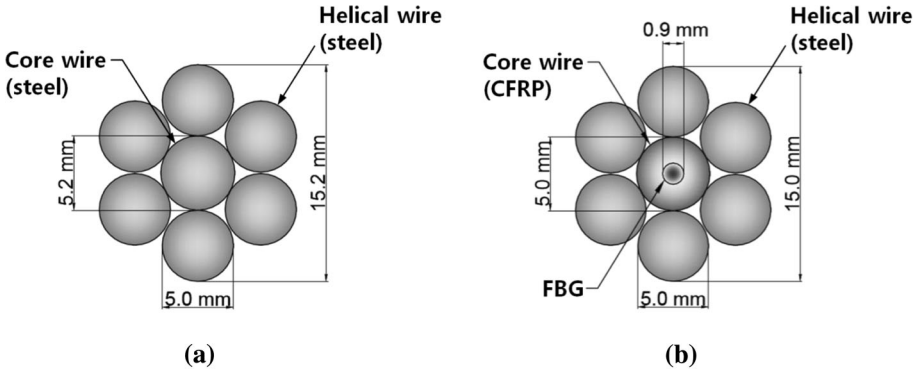

Fig. 2 Comparison of strands. **a** General strand, **b** smart strand.

not represent the actual axial strain because of the inclination of the helical wires and the difference of the length between the helical wire and the core wire. Damage of the lead wires required for this type of gauge during the insertion of strands into a sheath and during tensioning is another anticipated problem.

In order to address the aforementioned conventional problems, the Smart Strand with the embedded fiber Bragg grating (FBG) sensors was developed in this study as shown in Fig. 2b to accurately measure the strain and prestressing force along the strand (KICT 2013, 2014; Kim 2015; Kim et al. 2015). In the Smart Strand, the steel core wire of a general strand is replaced with carbon fiber reinforced polymer (CFRP) to contain the optical fiber and Bragg grating sensors at the center of the core wire section. Among the various possible ways to fabricate the CFRP, the braidtrusion method was adopted in the developed Smart Strand to prevent the galvanic corrosion that may occur due to the contact with the outer steel helical wires, by virtue of the coated nylon fiber (Kim et al. 2015). In comparison, some researchers developed FBG sensors embedded in an ordinary steel core wire (Kim et al. 2012). However, it was demonstrated that the CFRP core wire developed in this study is more advantageous than the steel core wire in terms

of mechanical property and the convenience in the fabrication and embedment of the optical fibers (KICT 2013). On the other hand, a different type of FRP and FBG sensing technique to that used in this study was employed in another study (Zhou et al. 2009).

Detail of the principle of the FBG sensor can be found in many references (Jang and Yun 2009; Kim et al. 2012; Nellen et al. 1999). FBG sensors have widely been used recently due to a number of advantages over the conventional sensing technique using electrical resistance, such as non-sensitivity to electromagnetic interference and tolerance for extremely low or high temperatures, etc. When light penetrates into an optical fiber, each Bragg grating embedded in the optical fiber reflects light waves that have a particular wavelength and transmits all other light waves. By analyzing the reflected light waves, the strain at the point of each Bragg grating can be obtained.

The mechanical properties of the CFRP core wire and the developed Smart Strand were verified through a number of specimen tests. Based on the stress–strain relationship curves of the Smart Strand, in addition to the sensing purposes, it was confirmed that the Smart Strand can be used even for structural purposes under service load and ultimate load conditions in most cases (KICT 2014; Kim 2015).

4. Full-Scale Test for Friction Coefficient

4.1 Test Specimen and Variables

Test variables were established to include various cases of PSC beams or girders constructed in practice. Test variables of the full-scale test of a PSC beam for evaluating friction coefficients are the diameter, curvature, and filling ratio of sheaths as shown in Table 2. Seven, twelve and nineteen strands are inserted into the sheath with 66, 85, and 100 mm diameters, respectively, in usual cases. However, the effect of the filling ratio on the friction coefficients was also taken into consideration by intentionally reducing the number of strands. In addition to the parabolically curved sheaths, straight sheaths were also arranged to separate the curvature effect from the wobble effect. The curvature shown in Table 2 does not refer to a mathematical curvature, but is defined by the sag of a curved sheath divided by the specimen length. Minor lateral curvature, which is inevitable when arranging many sheaths at mid-span, was ignored. The degree of the curvature of sheaths was determined by taking into account the ordinary curvature in PSC girder bridges, including box girders, and the intentionally increased curvature. Similar to an ordinary bonded post-tensioning system, the strands were not lubricated.

Figure 3 shows the 20 m long full-scale test specimen, where the height varies from 2.0 to 2.5 m to realize the largest curvature with an economical use of concrete. The specified compressive strength of the specimen is 40 MPa, which is the same as that of the standard PSC girders used in Korea. Also, self-consolidating concrete with a slump flow of 600 mm was used to accommodate the casting work and to ensure complete compaction of concrete, even in the case of congested sheaths and reinforcements.

The tendons were tensioned at only one end with the opposite end remaining as the dead end in order to increase friction loss and thus to purposely highlight the friction

Table 2 Test variables.

Category	Test variables	Values
Sheath	Diameter (mm)	66, 85, 100
	Curvature (sag/length)	0 (straight), 0.0295, 0.0490, 0.0785
	Material	Galvanized metal
Strand	Number	1, 7, 12, 13, 19
	Nominal diameter (mm)	15.2
	Ultimate strength (MPa)	1860
	Lubrication	Not applied

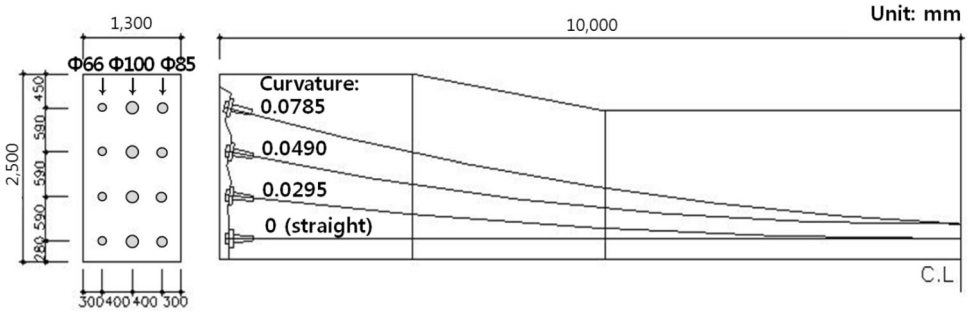

Fig. 3 Full-scale test specimen.

effect, although in practice, the tendons can also be tensioned at both ends. The jacking force per strand was increased by 20–30 MPa until it reached 180–200 kN, which nearly corresponds to the allowable tensile stress during jacking ($0.80f_{pu}$ or $0.94f_{py}$, where f_{pu}: Ultimate strength, and f_{py}: Yield strength) of the prestressing steel with an ultimate strength of 1860 MPa (ACI 2014; KCI 2012). A total of 13 Smart Strands were fabricated, where six strands have seven Bragg gratings (G1–G7 from dead end to live end) and the remaining seven strands have five Bragg gratings (G1–G5 from dead end to live end) that are equally spaced along the length. Among the total number of strands in one sheath, Smart Strands occupied some portion and normal strands occupied the remaining portion. The locations of the Smart Strands in the holes of the anchor head were determined so that various interactions related to the friction (between strands and between the strands and a sheath) can be accounted for. Figure 4 shows the arrangement of Smart Strands and normal strands in the case of the anchor head with 19 holes, corresponding to the sheath with a diameter of 100 mm and curvature of 0.0785 in Fig. 3. The figure also shows the sequence of work performed to investigate the effect of the filling ratio on friction coefficients.

In addition to the FBG sensors in the Smart Strands, extra measures were taken to complement or compare with the data obtained by the FBG sensors. First, a load cell was installed at the dead end to measure the total prestressing force at that location. Second, electro-magnetic (EM) sensors were installed immediately inside the jack, as shown in Fig. 5a, to measure the individual jacking force of the strands that reflects the jack loss (Cho et al. 2015). Third, electrical resistance gauges were attached to the strand surface corresponding to the selective locations of the FBG sensors. The dead end, i.e. the passive side of the strands, was realized by applying compressed grips as shown in Fig. 5b instead of normal wedges, to ensure reuse of the Smart Strands by minimizing the damage that may possibly be caused by the wedges. The optical fibers were connected to lead wires and a data logger by using a fusion splice.

4.2 Test Results

Figure 6 shows an example of the relationship between jacking force and strains obtained in one of the 19 strands (strand A in Fig. 4) inserted in a sheath with a diameter of 100 mm and curvature of 0.0785 from in Fig. 3. Strand A is an example of a Smart Strand with five Bragg gratings, while seven gratings were also applied for some other Smart Strands. Because the strands were tensioned up to less than the allowable stress, the strains are within an elastic range and thus are almost linearly proportional to the jacking force. It can also be identified in Fig. 6 that the Smart Strands can be utilized to check that the jacking force is correctly transmitted through the tendons.

The distribution of the prestressing force obtained at the same Smart Strand as that shown in Fig. 6 is presented in Fig. 7, where the values measured at the load cell, EM sensor, and jack are also indicated. The strains measured at the Bragg gratings of a Smart Strand can be converted to the prestress at each grating by multiplying the modulus of elasticity of the Smart Strand, and can further be converted to the prestressing force by multiplying the cross sectional

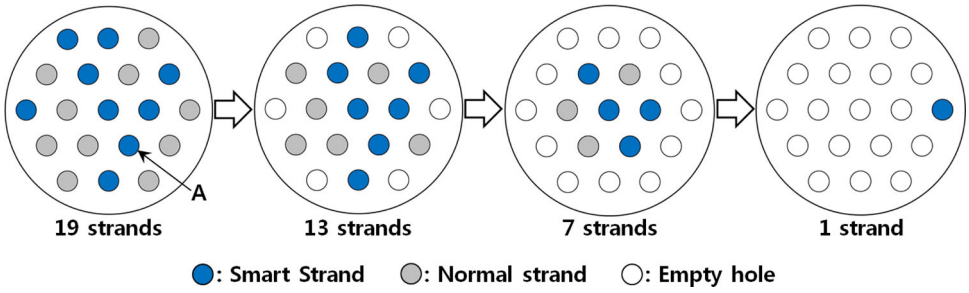

Fig. 4 Arrangement of strands in an anchor head with 19 holes.

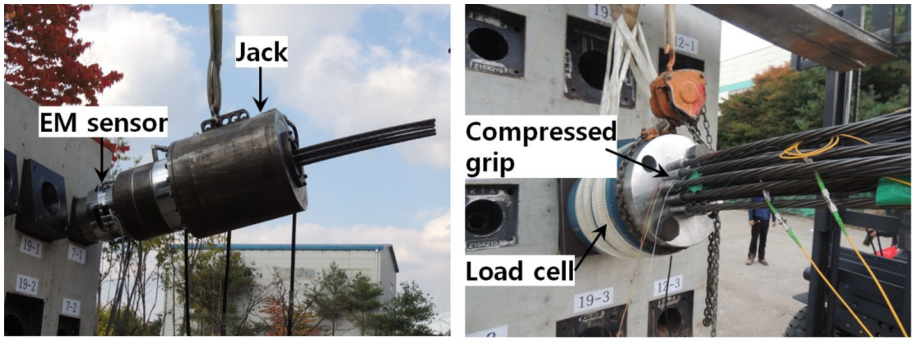

Fig. 5 Live and dead ends of test specimen. **a** Live end, **b** dead end.

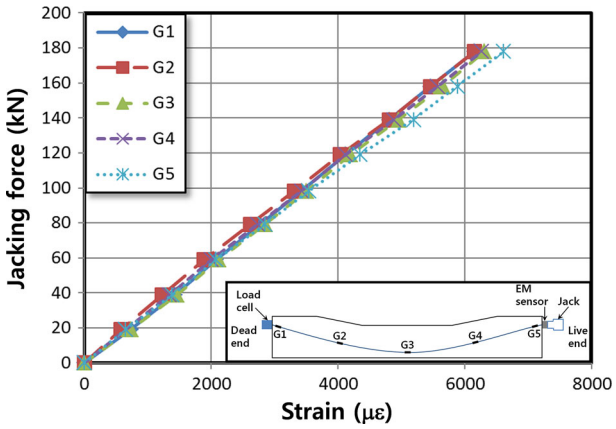

Fig. 6 Jacking force–strain relationship.

area of the Smart Strand. However, the computation of the prestressing force from the strain of the core wire of a Smart Strand can further be refined by accounting for the twist of helical wires and the difference of the cross sectional area and material property between the helical wires and the core wire as proposed in Eq. (2) (Cho et al. 2013; KICT 2013) in an analytical way. In a usual approximate calculation for a normal strand, $E_p = 2 \times 10^5$ MPa and $A_p = 138.7$ mm^2 are used to produce $E_pA_p = 27{,}740$ kN. On the other hand, the refined calculation for a Smart Strand using Eq. (2) results in $(E_pA_p)_{smart} = 26{,}007$ kN.

$$P = \left(f_c E_{p,c} A_{p,c} + f_h E_{p,h} A_{p,h}\right)\varepsilon_p = \left(E_p A_p\right)_{smart}\varepsilon_p \qquad (2)$$

where P is the prestressing force at the location of a Bragg grating, ε_p is the strain measured at a Bragg grating of a Smart Strand, f_c and f_h are the correction factors for core wire and helical wires, respectively, $E_{p,c}$ and $E_{p,h}$ are the modulus of elasticity of core wire and helical wires, respectively, $A_{p,c}$ and $A_{p,h}$ are the cross sectional area of core wire and helical wires, respectively, and $(E_pA_p)_{smart}$ is the equivalent E_pA_p for a Smart Strand.

It should be noted from Fig. 7 that the prestressing force of each strand can be separately determined in the Smart Strands and EM sensors in each load level (Lv. 1–Lv. 9), while only the averaged prestressing force in each strand can be obtained in the jack and load cell system by dividing the total force by the number of strands. This implies another advantage of the Smart Strands system; it can individually predict the distribution of the prestressing force of a specific strand. Therefore, the difference of the friction coefficients of each strand can be evaluated in the Smart Strands system, which can be used to investigate the variation of friction coefficients depending on the location of a strand inside the sheath. This shows a clear contrast to the conventional method where only the average friction coefficients can be derived inside a sheath using the elongation and jacking force measured at a jack, and the force measured at a load cell installed at the dead end, if available (Jeon et al. 2009). Also, it can be seen that the difference in prestressing forces between the EM sensor and the jack refers to the amount of jack loss that occurs due to the friction inside the jack.

5. Evaluation of Friction Coefficients

5.1 Methodology

Friction coefficients can be determined by applying the basic equation shown in Eq. (1) and the distribution of prestressing force as presented, for example, in Fig. 7. In this study, the friction coefficients were evaluated in two steps for sheaths with a specific diameter. First, the wobble friction coefficient was evaluated in the straight sheath. Since the variation of angle (α) does not exist in the straight sheath, the wobble friction coefficient (k) can be obtained from two prestressing forces (P_{x1} and P_{x2}) that were arbitrarily selected in a Smart Strand, judging from the form of Eq. (1), with the term of $\mu\alpha$ removed. The curvature friction coefficient (μ) can then be evaluated from Eq. (1) by applying two prestressing forces on a curved Smart Strand within a curved sheath with the wobble friction coefficient maintained as the previously obtained value for the straight sheath of the same diameter.

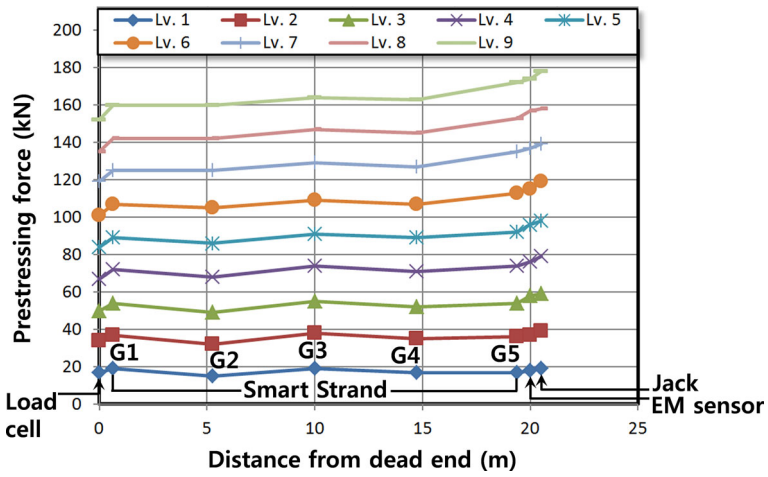

Fig. 7 Distribution of prestressing force.

As can be expected, the friction coefficients obtained in such a way vary depending on the two prestressing forces chosen. Therefore, a statistical approach is required to derive friction coefficients that are more reliable. During the statistical process, some of the friction coefficients may exhibit exceptionally high or low values when compared to the ordinary range of the coefficients shown in Table 1. This behavior can be attributed to the abnormal distribution of prestressing force that can occur in a local region due to an excessive twist of strands while inserting or jacking, or the inevitable irregularity of alignment of a sheath caused by insufficient support combined with the casting pressure of concrete. Therefore, data filtering has been performed for a minority of these exceptional values based on the upper or lower limits of the friction coefficients shown in Table 1. The filtering was performed in two different ways and the results are compared. The first case is based on the two Korean design codes; Structural Concrete Design Code (KCI 2012) and Design Code for Highway Bridges (KRTA 2010). Therefore, the wobble and curvature friction coefficients that were calculated outside the range of 0.0015–0.0066/m and 0.15–0.25/radian, respectively, have been excluded from the statistics. It can be identified that the values of friction coefficients of ACI 318-08 (ACI 2008) are almost identical to those of the Korean design codes. In the second case, the entire provisions in Table 1 were accounted for and, as a result, the effective range was extended to 0.00066–0.0066/m and 0.14–0.30/radian for the wobble and curvature friction coefficients, respectively.

When Eq. (1) is used to evaluate the friction coefficients, any two arbitrary prestressing forces measured at different points can be adopted, regardless of where they are measured among the Smart Strand, load cell, EM sensor, and jack. In this respect, two different approaches were employed in this study. First, two prestressing forces corresponding to the jack and one of the gratings in a Smart Strand were referred to. As mentioned previously, however, the prestressing force measured at the jack is only an average value and does not represent the exact prestressing force of the strand under consideration. Furthermore, although friction loss may also occur inside the jack and at the anchorage devices, the jacking force does not include these losses. These are the sources that may lower the accuracy of the resulting friction coefficients. In order to cope with these problems, in the second method, two prestressing forces obtained purely in two gratings of a Smart Strand were employed.

In the above evaluation process of friction coefficients, the accurate calculation of the distance and the variation of angle between two points is needed. The distance between two arbitrary points of Bragg grating can be easily calculated, since the gratings are embedded at equal spaces along the strands. The variation of angle can be calculated by measuring the angle formed between two tangent lines drawn from the two grating points. In order to perform this calculation, the following mathematical equation, Eq. (3) (Kreyszig 2011), for calculating the length of a curve is required to inversely obtain the horizontal distance, i.e. x coordinate, corresponding to the grating point. The curved form of a sheath is assumed to be a parabola, as has frequently been assumed in design practice.

$$l = \int_a^b \sqrt{1 + (f'(x))^2}\,dx \tag{3}$$

where l is the length of the partial curve of $f(x)$ between $x = a$ and $x = b$, and $f(x)$ is the shape of a sheath assumed as a parabola.

5.2 Analysis Results

The results of the statistical analyses are presented in Figs. 8 and 9 for wobble and curvature friction coefficients, respectively. In these figures, 'jack-grating' implies that the jacking force and prestressing force at a grating were used for analysis, while 'grating-grating' indicates that two prestressing forces obtained at two gratings were adopted. Also, 'Korean provisions' and 'entire provisions' imply that the statistical data were filtered based on the limit of the two Korean design codes (KCI 2012; KRTA 2010) and entire provisions shown in Table 1, respectively.

The average wobble and curvature friction coefficients of the cases shown in Figs. 8 and 9 were evaluated as 0.0038/m and 0.21/radian, respectively. Therefore, the wobble friction coefficient was slightly smaller than the average value of 0.0041/m in the Korean design codes (KCI 2012; KRTA 2010), while the curvature friction coefficient was a little larger than the average value of 0.2/radian in the Korean design codes. In general, however, the evaluated values were close to the average values specified in the Korean design codes. Also, it can be observed that, in each pair of the wobble and curvature friction coefficients, if the wobble friction coefficient is increased, the corresponding curvature friction coefficient decreases, and vice versa. This can be expected as a matter of course because the two coefficients are interrelated in Eq. (1). The difference of the values in each group, i.e. jack-grating or grating–grating, is due to the difference of the range used for data filtering.

In most of the previous studies using the strands with FBG sensors, only the distribution of prestressing force considering prestress losses was estimated, and the friction coefficients were not derived (Kim et al. 2012; Xuan et al. 2009; Zhou et al. 2009). At most, the distribution of prestressing force obtained by assuming different friction coefficients was compared with the measured data (Kim et al. 2012). The research significance of this study can be found in a direct evaluation of the friction coefficients by utilizing the advanced sensing technology using FBG embedded in a strand. When the scope is extended to the previous studies for proposing friction coefficients, regardless of which method is adopted, the coefficients show a wide range of variation depending on the methodology used (Gupta 2005; Jeon et al. 2009; Kim et al. 2012; Kitani and Shimizu 2009; Moon and Lee 1997) and consistent coefficients have not yet been established. Another factor for this large variation may be the difference in material and workmanship in each study. For example, the degree of wobble friction sensitively varies according to the supporting interval, stiffness, and surface

condition of a sheath and to the workmanship dedicated to maintain the original shape of a sheath during the installation of the sheath and the casting of concrete.

The confidence level of each friction coefficient was also investigated as shown in Figs. 8 and 9. The 95 % confidence interval was calculated using the corresponding mathematical equation (Kreyszig 2011) for each method, by assuming normal distribution of the data. Although each method has a narrower band of the confidence interval, the 95 % confidence interval marked with dotted lines in Figs. 8 and 9 only presents the absolute lower and upper limits that can cover all cases with sufficient reliability. Through this type of statistical method, the wide range of the friction coefficients specified in a specific provision can be reduced to enhance the accuracy and reliability. For example, while the range of the vertical axes shown in Figs. 8 and 9 corresponds to that of ACI 318-08 (ACI 2008) and Korean design codes (KCI 2012; KRTA 2010), the range can be narrowed to 0.0021–0.0058/m and 0.178–0.244/radian for wobble and curvature friction coefficients, respectively, by applying a 95 % confidence level. This means that the range was reduced by 27 and 34 % for the wobble and curvature friction coefficients in this study, respectively, which may accommodate the choice of friction coefficients for field engineers and designers.

5.3 Discussion

As mentioned earlier, a number of conventional electrical resistance strain gauges were also implemented in this study for comparison with the Smart Strand system. As has been frequently reported, however, a large number of electrical resistance strain gauges were made unavailable due to the damage of sensors and lead wires during insertion of strands into a sheath and during tensioning. The strains measured by Smart Strands were compared with those measured by the remaining electrical resistance gauges attached to the surface

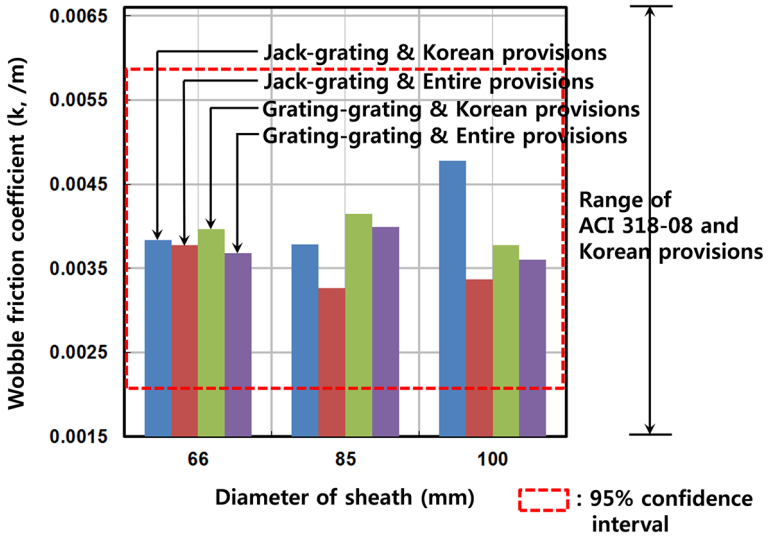

Fig. 8 Wobble friction coefficient.

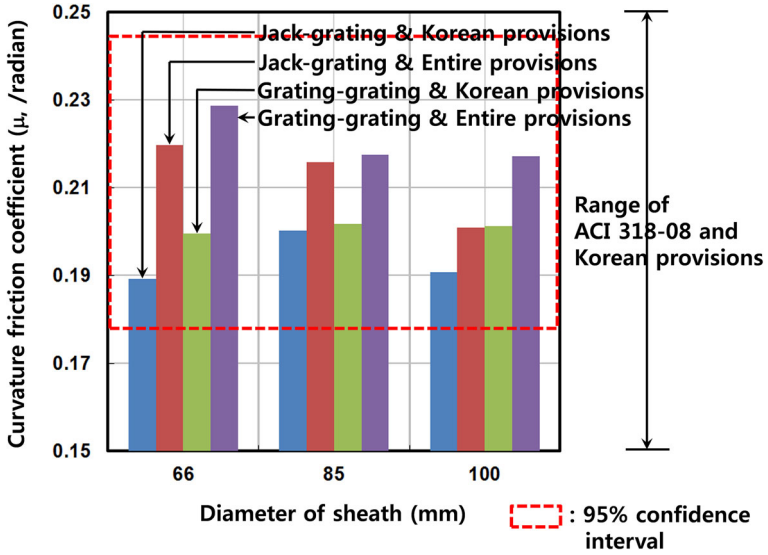

Fig. 9 Curvature friction coefficient.

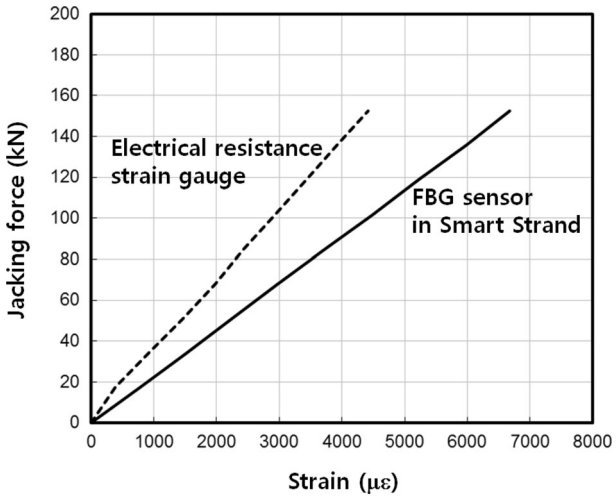

Fig. 10 Comparison of strains of a strand.

of helical wires, corresponding to the same grating points. The data obtained using electrical resistance gauges showed a great amount of difference from those of Smart Strands, since the electrical resistance gauges may be sensitively affected by such factors as the alignment of the gauges on the helical wires and the workmanship related to the proper bonding of the gauges. In the overall trend, the strains of the conventional gauges were smaller than those of Smart Strands by 20–30 % as representatively shown in Fig. 10. The difference between the strains can be attributed to the difference in the length between the core wire and helical wire, and the slope of the helical wire with respect to the core wire (8.2°), etc. For example, the longer length of the helical wire wound around the core wire can result in a smaller strain. The difference in the actual stresses between the core wire and helical wire has also been investigated by Cho et al. (2013). Therefore, the strains measured using electrical resistance gauges should be interpreted with special care, especially when applied to the strands, although they are still widely used.

In this study, the effect of curvature, diameter, and filling ratio of a sheath, and the effect of the location of a strand in a sheath on the friction coefficients have also been investigated. However, these topics will be dealt with in another paper since they involved extensive analyses. This study presented the general average friction coefficients in terms of wobble and curvature, taking into consideration all the test variables, since the friction coefficients are specified without any limited condition in most provisions as shown in Table 1.

6. Conclusions

In order to overcome the various drawbacks of the existing measurement system of the prestressing force of strands in PSC structures, the Smart Strand system was developed in this study by devising a core wire made of carbon fiber reinforced polymer with the fiber Bragg grating sensors embedded. As one of the applications of the Smart Strand, friction coefficients were evaluated using the strain distribution of strands obtained from the full-scale test of a 20 m long beam. Based on the results of the above investigation, the following conclusions can be drawn:

(1) The tests were performed for various curvatures, diameters, and filling ratios of a sheath and for various strand locations inside a sheath to include general cases. The analysis results showed the wobble and curvature friction coefficients of 0.0038/m and 0.21/radian on average, respectively, for general galvanized metal sheaths. These values correspond to the values within the middle of the range specified in ACI 318-08 in the U.S. and Structural Concrete Design Code in Korea.

(2) A wide range of friction coefficients specified in the general provisions may cause some difficulty and trial-and-error in choosing an appropriate coefficient for design purposes. Through statistical analyses using a confidence interval, the accuracy of the coefficients was improved by reducing the effective range. For example, the ranges in ACI 318-08 in the U.S. and Structural Concrete Design Code in Korea were reduced by 27–34 %.

(3) The strains measured using conventional electrical resistance strain gauges showed a great amount of difference from those of Smart Strands. In the overall trend, the strains of conventional gauges were smaller than those of Smart Strands by 20–30 %. The differences in the strains may originate from the differences in the length between the core wire and helical wire, and the slope of the helical wire with respect to the core wire, etc. Therefore, the strains measured using electrical resistance gauges should be interpreted with special care in terms of the strains of the strands.

(4) The effect of curvature, diameter, and filling ratio of a sheath, and the effect of the location of a strand in a sheath on the friction coefficients were also investigated, but these will be dealt with in another paper as further study. By applying the Smart Strand system to reliably estimate the distribution of the prestressing force of strands, as has been demonstrated in this study, relevant provisions regarding the design of PSC structures can be verified and improved, if necessary. It is also expected that the Smart Strand system will be used for the maintenance or management of PSC structures by the long-term monitoring of prestressing force.

Acknowledgments

This research was supported by a grant from a Strategic Research Project (Development of Smart Prestressing and Monitoring Technologies for Prestressed Concrete Bridges) funded by the Korea Institute of Civil Engineering and Building Technology.

Open Access

References

ACI Committee 318. (2008). *Building code requirements for structural concrete (ACI 318-08)*. Farmington Hills, MI, US: American Concrete Institute (ACI).

ACI Committee 318. (2014). *Building code requirements for structural concrete (ACI 318-14)*. Farmington Hills, MI, US: American Concrete Institute (ACI).

American Association of State Highway and Transportation Officials (AASHTO). (2002). *Standard specifications for highway bridges* (17th ed.). Washington, D.C., US: AASHTO.

American Association of State Highway and Transportation Officials (AASHTO). (2014). *AASHTO LRFD bridge design specifications* (7th ed.). Washington, D.C., US: AASHTO.

American Society for Testing and Materials (ASTM). (2012). *Standard specification for steel strand, uncoated seven-wire for prestressed concrete (ASTM A416/A416M-12a)*. West Conshohocken, PA, US: ASTM.

British Standards Institution (BSI). (1997). *Structural use of concrete (BS 8110)*. London, UK: BSI.

Canadian Standards Association (CSA). (2006). *Canadian highway bridge design code, CAN/CSA-S6* (10th ed.). Mississauga, ON, Canada: CSA.

Cho, K. H., Kim, S. T., Park, S. Y., & Park, Y. H. (2013). Computation of the strand resistance using the core wire strain measurement. *Engineering, 5*, 850–855.

Cho, K. H., Park, S. Y., Cho, J. R., Kim, S. T., & Park, Y. H. (2015). Estimation of prestress force distribution in the multi-strand system of prestressed concrete structures. *Sensors, 15*, 14079–14092.

Euro-International Committee for Concrete (CEB). (1993). *CEB-FIP model code*. Lausanne, Switzerland: Thomas Telford Services Ltd.

European Committee for Standardization (CEN). (2002). *Design of concrete structures (Eurocode 2)*. Brussels, Belgium: CEN.

Gupta, P. R. (2005). *Rational determination of friction losses in post-tensioned construction* (pp. 129–144). SP-231, American Concrete Institute (ACI).

Jang, I. Y., & Yun, Y. W. (2009). Study on stress transfer property for embedded FBG strain sensors in concrete monitoring. *International Journal of Concrete Structures and Materials, 3*(1), 33–37.

Japan Road Association (JRA). (2012). *Specifications for highway bridges-Part III. Concrete bridges*. Tokyo, Japan: JRA.

Japan Society of Civil Engineers (JSCE). (2007). *Standard specifications for concrete structures-design*. Tokyo, Japan: JSCE.

Jeon, S. J., Park, J. C., Park, I. K., & Shim, B. (2009). Estimation of friction coefficients based on field data. *Journal of the Korean Society of Civil Engineers, 29*(5A), 487–494.

Jeung, B. K., Han, K. B., & Park, S. K. (2000). An experimental study on the frictional loss of stress in the prestressing tendons. *Journal of the Korean Society of Civil Engineers, 20*(5-A), 797–804.

Kim, S. H. (2015). *An experimental study on measurement of friction coefficient using smart strand*. Master's thesis, Ajou University, Suwon-si, Korea.

Kim, J. M., Kim, H. W., Park, Y. H., Yang, I. H., & Kim, Y. S. (2012). FBG sensors encapsulated into 7-wire steel strand for tension monitoring of a prestressing tendon. *Advances in Structural Engineering, 15*(6), 907–917.

Kim, S. T., Park, Y. H., Park, S. Y., Cho, K. H., & Cho, J. R. (2015). A sensor-type PC strand with an embedded FBG sensor for monitoring prestress forces. *Sensors, 15*, 1060–1070.

Kitani, T., & Shimizu, A. (2009). Friction coefficient measurement test on 13MN class tendon of PC strands for prestressed concrete containment vessel (PCCV). In: *Proceedings of 20th international conference on structural mechanics in reactor technology (SMiRT 20)*, Paper 1825.

Korea Concrete Institute (KCI). (2012). *Structural concrete design code*. Seoul, Korea: KCI.

Korea Institute of Civil Engineering and Building Technology (KICT). (2013). *Development of smart prestressing and monitoring technologies for prestressed concrete bridges, KICT 2013-167*. Goyang-si, Korea: KICT.

Korea Institute of Civil Engineering and Building Technology (KICT). (2014). *Development of smart prestressing and monitoring technologies for prestressed concrete bridges, KICT 2014-171*. Goyang-si, Korea: KICT.

Korea Road and Transportation Association (KRTA). (2010). *Design code for highway bridges*. Seoul, Korea: KRTA.

Korean Agency for Technology and Standards (KATS). (2011). *Uncoated stress-relieved steel wires and strands for prestressed concrete (KS D 7002)*. Seoul, Korea: Korean Standards Association (KSA).

Kreyszig, E. (2011). *Advanced engineering mathematics* (10th ed.). Hoboken, NJ, US: Wiley.

Moon, J. K., & Lee, J. H. (1997). A study on the determination of prestressing force considering frictional loss in PS concrete structures. *Journal of the Korean Society of Civil Engineers, 17*(I-1), 89–99.

Nellen, P. M., Frank, A., Broennimann, R., Meier, U., & Sennhauser, U. J. (1999). Fiber optical Bragg grating sensors embedded in CFRP wires. *SPIE Proceedings, 3670*, 440–449.

Nilson, A. H. (1987). *Design of prestressed concrete* (2nd ed.). Hoboken, NJ, US: Wiley.

Park, Y. H., & Gil, H. B. (2004). An error analysis of the friction assessment method for PS tensioning. In: *Proceedings of Korean Society of Civil Engineers (KSCE) conference*, pp. 106–111.

Park, Y. H., & Kang, H. T. (2003). A criterion for application of friction assessment methods in PS tensioning management. In: *Proceedings of Korean Society of Civil Engineers (KSCE) conference*, pp. 594–599.

Post-Tensioning Institute (PTI). (2006). *Post-tensioning manual* (6th ed.). Phoenix, AZ, US: PTI.

Precast/Prestressed Concrete Institute (PCI). (2011). *Bridge design manual* (3rd ed.). Chicago, IL, US: PCI.

State of California Department of Transportation (Caltrans) Engineering Services. (2005). *Prestress manual*. Sacramento, CA, US: Caltrans.

The International Federation for Structural Concrete (fib). (2013). *fib model code for concrete structures 2010*. Lausanne, Switzerland: fib.

Xuan, F. Z., Tang, H., & Tu, S. T. (2009). In situ monitoring on prestress losses in the reinforced structure with fiber-optic sensors. *Measurement, 42*, 107–111.

Zhou, Z., He, J., Chen, G., & Ou, J. (2009). A smart steel strand for the evaluation of prestress loss distribution in post-tensioned concrete structures. *Journal of Intelligent Material Systems and Structures, 20*, 1901–1912.